Automated classification of brain tissue

Comparison between hyperspectral imaging and diffuse reflectance spectroscopy

Lai, Marco; Skyrman, Simon; Shan, Caifeng; Paulussen, Elvira; Manni, Francesca; Swamy, Akash; Babic, Drazenko; Edstrom, Erik; Persson, Oscar; Burstrom, Gustav

DOI
10.1117/12.2548754

Publication date
2020

Document Version
Final published version

Published in
Medical Imaging 2020

Automated classification of brain tissue: comparison between hyperspectral imaging and diffuse reflectance spectroscopy

Lai, Marco, Skyrman, Simon, Shan, Caifeng, Paulussen, Elvira, Manni, Francesca, et al.

Marco Lai, Simon Skyrman, Caifeng Shan, Elvira Paulussen, Francesca Manni, Akash Swamy, Drazenko Babic, Erik Edstrom, Oscar Persson, Gustav Burstrom, Adrian Elmi-Terander, Benno H. W. Hendriks, Peter H. N. de With, "Automated classification of brain tissue: comparison between hyperspectral imaging and diffuse reflectance spectroscopy," Proc. SPIE 11315, Medical Imaging 2020: Image-Guided Procedures, Robotic Interventions, and Modeling, 113151X (16 March 2020); doi: 10.1117/12.2548754

SPIE.

Event: SPIE Medical Imaging, 2020, Houston, Texas, United States

Automated classification of brain tissue: comparison between hyperspectral imaging and diffuse reflectance spectroscopy

Marco Lai[a,b], Simon Skyrman[c], Caifeng Shan[a], Elvira Paulussen[a], Francesca Manni[b], Akash Swamy[a,d], Drazenko Babic[a], Erik Edstrom[c], Oscar Persson[c], Gustav Burstrom[c], Adrian Elmi-Terander[c], Benno H.W. Hendriks[a,d], and Peter H.N. de With[d]

[a]Philips Research, High Tech Campus, Eindhoven, The Netherlands
[b]Eindhoven University of Technology (TU/e), Eindhoven, The Netherlands
[c]Department of Neurosurgery, Karolinska University Hospital and Department of Clinical Neuroscience, Karolinska Institutet, Stockholm, Sweden
[d]Department of Biomechanical Engineering, Delft University of Technology, Mekelweg 2, 2628 CD, Delft, the Netherlands

ABSTRACT

In neurosurgery, technical solutions for visualizing the border between healthy brain and tumor tissue is of great value, since they enable the surgeon to achieve gross total resection while minimizing the risk of damage to eloquent areas. By using real-time non-ionizing imaging techniques, such as hyperspectral imaging (HSI), the spectral signature of the tissue is analyzed allowing tissue classification, thereby improving tumor boundary discrimination during surgery. More particularly, since infrared penetrates deeper in the tissue than visible light, the use of an imaging sensor sensitive to the near-infrared wavelength range would also allow the visualization of structures slightly beneath the tissue surface. This enables the visualization of tumors and vessel boundaries prior to surgery, thereby preventing the damaging of tissue structures. In this study, we investigate the use of Diffuse Reflectance Spectroscopy (DRS) and HSI for brain tissue classification, by extracting spectral features from the near infra-red range. The applied method for classification is the linear Support Vector Machine (SVM). The study is conducted on ex-vivo porcine brain tissue, which is analyzed and classified as either white or gray matter. The DRS combined with the proposed classification reaches a sensitivity and specificity of 96%, while HSI reaches a sensitivity of 95% and specificity of 93%. This feasibility study shows the potential of DRS and HSI for automated tissue classification, and serves as a first step towards clinical use for tumor detection deeper inside the tissue.

Keywords: Hyperspectral imaging, diffuse reflectance spectroscopy, neurosurgery, brain surgery, image-guided surgery, machine learning, image classification, tissue classification

1. INTRODUCTION

Technical aids to delineate tumor margins and distinguish between healthy brain and tumor are of great value for neurosurgeons. Neuro-navigation and fluorescent tumor markers, as well as imaging techniques such as intra-operative Magnetic Resonance Imaging (ioMRI) and intra-operative CT, are commonly used for this purpose. However, there are several limitations due to brain shift and low spatial resolution.[1] The use of a real-time non-ionizing imaging techniques would allow analyzing the spectral signature of the tissue and therefore making a tissue classification, to aid during surgery. Since infrared light penetrates deeper in the tissue rather than visible light, the use of an imaging sensor sensitive to the near-infrared wavelength range would enable the visualization of sub-surface structures and minimize the risk of tissue damage. In Diffuse Reflectance Spectroscopy (DRS),[2] tissue is probed by sending white light from a broadband light source through an optical fiber. After the light has interacted with the tissue, another optical fiber is used to collect the diffusely reflected light. The light is then analyzed, and the spectral signature is used for distinguishing between different tissue types.[3,4]

Further author information: (Send correspondence to Marco Lai)
Marco Lai: E-mail: marco.lai@philips.com

Medical Imaging 2020: Image-Guided Procedures, Robotic Interventions, and Modeling, edited by Baowei Fei, Cristian A. Linte, Proc. of SPIE Vol. 11315, 113151X · © 2020 SPIE
CCC code: 1605-7422/20/$21 · doi: 10.1117/12.2548754

DRS has been shown to be able to estimate the concentration of blood, fat, and other optical properties in various clinical applications, such as tumor and nerve detection. Hyperspectral Imaging (HSI) is an emerging imaging modality for medical applications with the potential of for non-invasive disease diagnosis and surgical guidance.[5] The objective of hyperspectral imaging is to collect a three-dimensional dataset of spatial and spectral information, known as hypercube.[6] With this information, it is possible to obtain a spectral signature of each imaged pixel.[7,8] Preliminary research demonstrates that HSI has potential for providing diagnostic information for various diseases, when combining it with Machine Learning (ML) methods in a broad sense, which include the well-known Support Vector Machine (SVM) and Convolutional Neural Networks (CNNs).[9,10]

In this feasibility study, a hyperspectral endoscopy imaging system has been designed that couples a mosaic sensor exploiting 25 wavelength bands, with a rigid endoscope. Using this system, we have investigated the applicability of HSI and DRS for brain tissue classification, extracting spectral features from the near infra-red range. The applied method for classification is the linear Support Vector Machine (SVM). The study is conducted on eight *ex-vivo* porcine brain-tissue samples, which are analyzed and classified as either white or gray matter.

2. METHOD

Figure 1 shows the framework applied for training and testing. First, the hyperspectral images and DRS signals, acquired on white and gray matter using the color image as a reference, are preprocessed to perform data normalization and noise reduction. Second, relevant features are extracted and used for classification. Eventually, leave-one-out cross-validation (LOOCV) testing is applied to avoid overfitting.

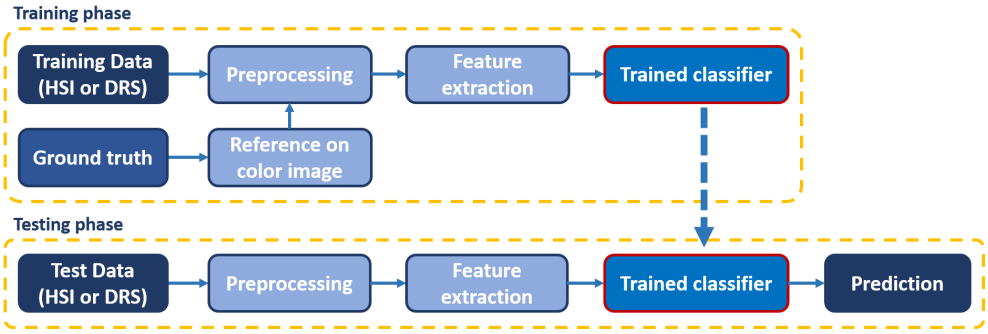

Figure 1: Method used for training and classification in the system.

2.1 HSI system

The HSI system is composed of a mosaic sensor, coupled to a rigid endoscope via an endoscopic camera coupler with a focal length of 35 mm. The hyperspectral sensor is a CMOS Snapshot Mosaic device called SNm5×5 NIR (near-infrared) sensor (IMEC, Leuven, Belgium), which integrates spectral filters per pixel monolithically on top of the imager wafers in a mosaic pattern. This solution is one of the first commercial systems, offering true multispectral imaging at video rates in a small form factor. The sensor is capturing 25 spectral bands, from 676 to 954 nm, with a collimated spectral bandwidth of less than 15 nm and 10-bit color depth. The sensor has a resolution of 2050×1080 pixels, while the 25 bands are arranged in a 5×5 mosaic grid. This results in achieving an imaging pixel resolution of 410×216 pixels for each of the 25 bands. The hyperspectral sensor is mounted in a vertical position on a rigid frame, to image the specimens placed on the horizontal plane (Figure 2a). Specimens are illuminated by the light transmitting system of the endoscope, with light covering the sensitive range of the sensor.

2.2 DRS system

The experimental setup for DR spectral acquisition consists of a tungsten halogen broadband light source (360 to 2500 nm) with an optical spectrometer (depicted in Figure 2b). A fiber-optic probe of 1.6 mm was used. The probe contains two optic fibers, with a 1.22 mm center-to-center distance between them and axis of symmetry

parallel to the axis of symmetry of the probe. One fiber is connected to the tungsten halogen broadband light source and the second fiber is connected to the spectrometer (Andor Technology, DU420ABRDD), with a spectral response from 400 to 1600 nm. LabVIEW software (National Instruments, Austin, Texas) developed in-house was used to control the spectrometer and acquire the data.

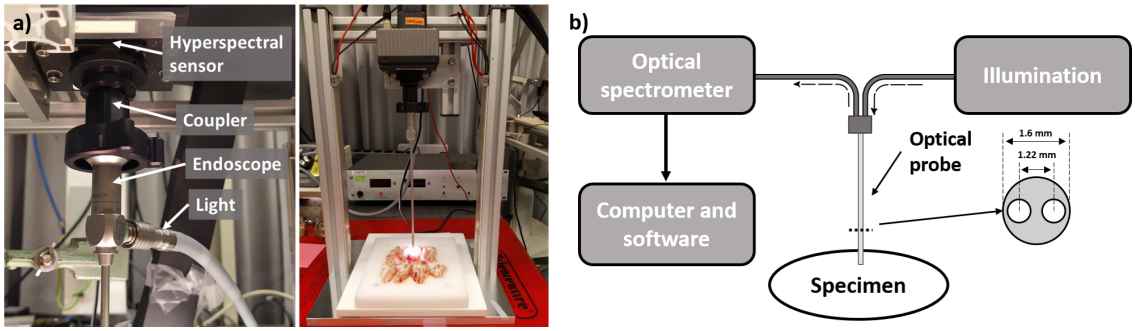

Figure 2: a) Photo of the system designed for hyperspectral imaging; b) Schematic of the system used for diffuse reflectance spectroscopy.

2.3 Data acquisition

In this study, eight *ex-vivo* porcine brain-tissue samples were scanned using the hyperspectral and DRS sensors. Brain samples were gathered at the LifeTec Group (Eindhoven, The Netherlands) and included in this study. All ethical guidelines for *ex-vivo* animal studies were followed. The porcine brain specimens were cut in coronal slices and pictured with a color camera (Figure 3a). For each tissue slice, the DRS signals for the white and the gray matter were acquired, using the color image as a reference, where the DRS capturing locations were annotated on the color image (Figure 3b). Then, the hyperspectral imaging acquisitions were performed. Each slice was imaged with HSI multiple times, acquiring images from different spots on the same slice. Afterwards, hyperspectral images were manually registered on the color image (Figure 3c). On each of the eight porcine brain specimens, about 140 DRS signals (70 for the white matter and 70 for the gray) and about 25 hyperspectral images were acquired.

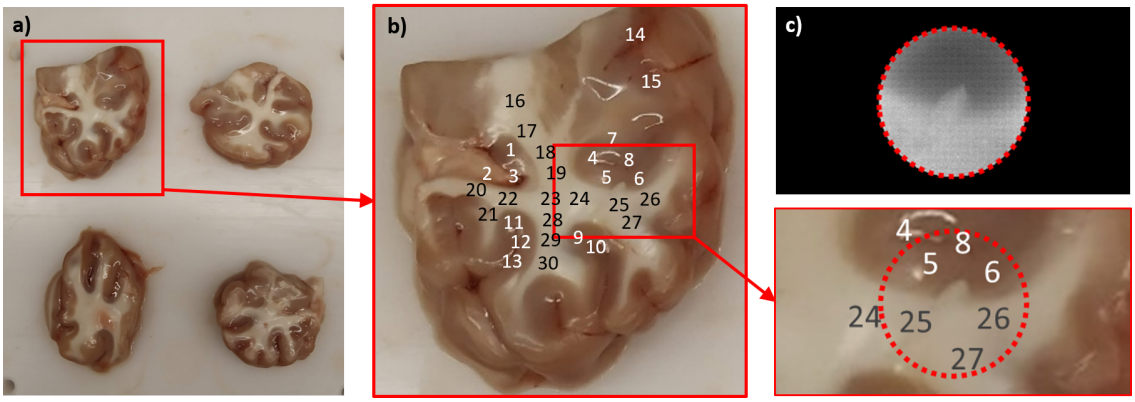

Figure 3: a) Porcine brain was cut in coronal slices; b) Brain slice annotated with the locations of the DRS acquisitions; c) Hyperspectral image acquired on a portion of the brain slice and manually registered on the color image.

2.4 Data preprocessing and feature extraction

The hyperspectral images and the DRS signals are calibrated and preprocessed, to achieve data normalization and noise reduction, which does significantly affect the classification accuracy. Calibration for HSI, based on

Lu *et al.*,[11] is achieved at each wavelength λ sampled for all pixels i, j of the HSI, by subtracting the inherent dark current and dividing by a white reference, as specified by:

$$I_{\text{cal}}(\lambda, i, j) = \frac{I_{\text{raw}}(\lambda, i, j) - I_{\text{dark}}(\lambda, i, j)}{I_{\text{white}}(\lambda, i, j) - I_{\text{dark}}(\lambda, i, j)}, \tag{1}$$

where I_{cal} denotes the calibrated reflectance value, I_{raw} is the effective measured diffuse reflectance value at the given pixel, I_{white} the intensity value for the white reference, acquired by positioning a white reference plate in the field of view, and I_{dark} represents the dark reference value, acquired by keeping the camera shutter closed. DRS signals are calibrated in a similar way, giving

$$S_{\text{cal}}(\lambda) = \frac{S_{\text{raw}}(\lambda) - S_{\text{dark}}(\lambda)}{S_{\text{white}}(\lambda) - S_{\text{dark}}(\lambda)}, \tag{2}$$

where S_{cal} represents the calibrated reflectance value, S_{raw} is the effective measured diffuse reflectance value at each λ, S_{white} denotes the intensity value for the white reference, acquired by positioning a white reference plate in front of the probe, and S_{dark} the dark reference value, acquired by shuttering the light input.

Then, since the hyperspectral-imaging sensor is operational in 25 wavelength bands, we match the dimension of the DRS signals to select the same 25 bands. Afterwards, the hyperspectral images are segmented according to the DRS signals annotated on the color images and then averaged, to obtain the same spatial density of information for DRS signals. We exploited the assumption that an area of uniform pixel intensity in the HSI image corresponds to the same type of tissue of the color image (Figure 4). This approach also increases the robustness of the spectral noise for HSI. Eventually, the DRS and HSI signals are normalized with respect to the value of the first wavelength band (676 nm). This allows removing the dependence on absolute intensity values and therefore to classify the signals only according to the signal shape. The normalized value of HSI and DRS signals and their derivative are used for the classification.

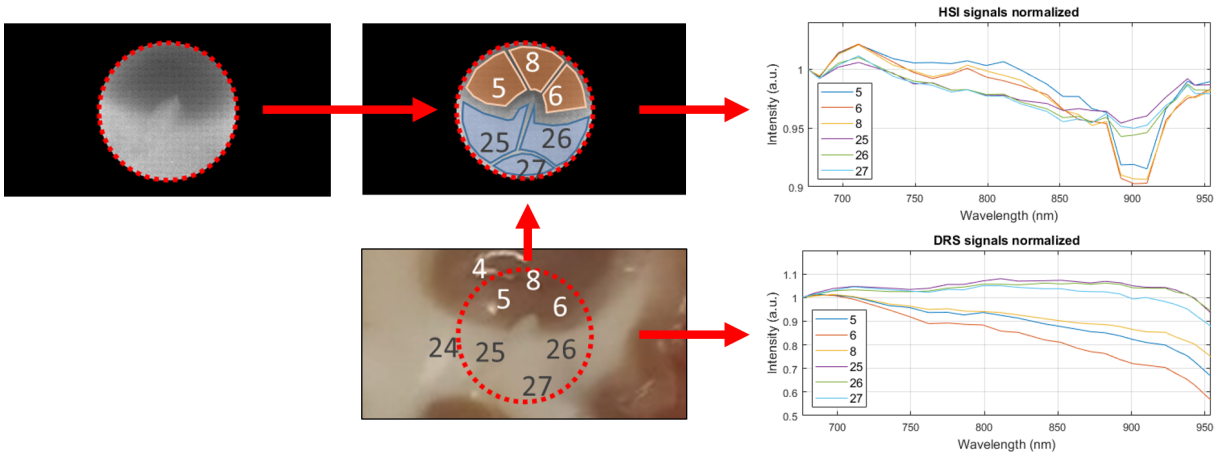

Figure 4: HSI segmentation according to the DRS signals annotation on the color image. The plots show the HSI and DRS signals, respectively, acquired on the same locations.

2.5 Classification of HSI and DRS data and validation

For this feasibility study, a supervised learning approach is adopted, employing a linear SVM , to design predictive models for tissue classification from HSI and DRS acquisitions. Leave-one-out cross-validation testing is applied. That means that the classifier is trained for each of the eight brain samples, using all the data except for one sample that is used for testing. This process avoids double-sample usage and prevents overfitting. After classification, each signal is labeled as white or gray matter tissue. As a result, we obtain binary classified images for each brain sample.

To evaluate the classifier performance, we have computed the receiver operating characteristics (ROC) curve, area under the curve (AUC), sensitivity (Se) and specificity (Sp). The last two metrics measure the signals correctly classified as white (Se) and as gray (Sp), respectively, as defined in equations from literature, based on TN: true negatives, TP: true positives, FP: false positives, and FN: false negatives. For benchmarking, the same performance metrics of sensitivity and specificity are exploited during the validation process, which are specified by:

$$Se = \frac{TP}{TP + FN}, \qquad \text{and} \qquad Sp = \frac{TN}{TN + FP}. \tag{3}$$

3. EXPERIMENTAL RESULTS

Figure 5 shows the averaged normalized signals of white and gray matter of the eight brain samples, both for DRS and HSI. DRS signals are smoother and more consistent among each other with respect to HSI signals, both for white and gray matter. For the gray matter, DRS curves show a constant decrease in reflectance value, from 676 nm to 954 nm. Instead, HSI shows relative flat curves, which suddenly drop in the range of 900 nm and after that start rising again. This trend is different for Sample 3, 4 and 6, where an unexpected increase in reflectance occurs between 840 and 870 nm before the drop at 900 nm. For the white matter, DRS curves are almost flat and then the reflectance drops after 900 nm. For HSI, curves smoothly decrease until 900 nm and then increase slightly again. This does not hold for Sample 3 and 6, which show a slight increase of reflectance between 840 and 870 nm, as for their respective curves of gray matter. Figure 6 depicts the ROC curves of the detection rates. The AUC values, sensitivity (Se) and specificity (Sp) are shown in Table 1. For DRS, sensitivity, specificity and AUC all reach 96%, where for HSI, sensitivity reaches 95%, specificity 93% and AUC 95%.

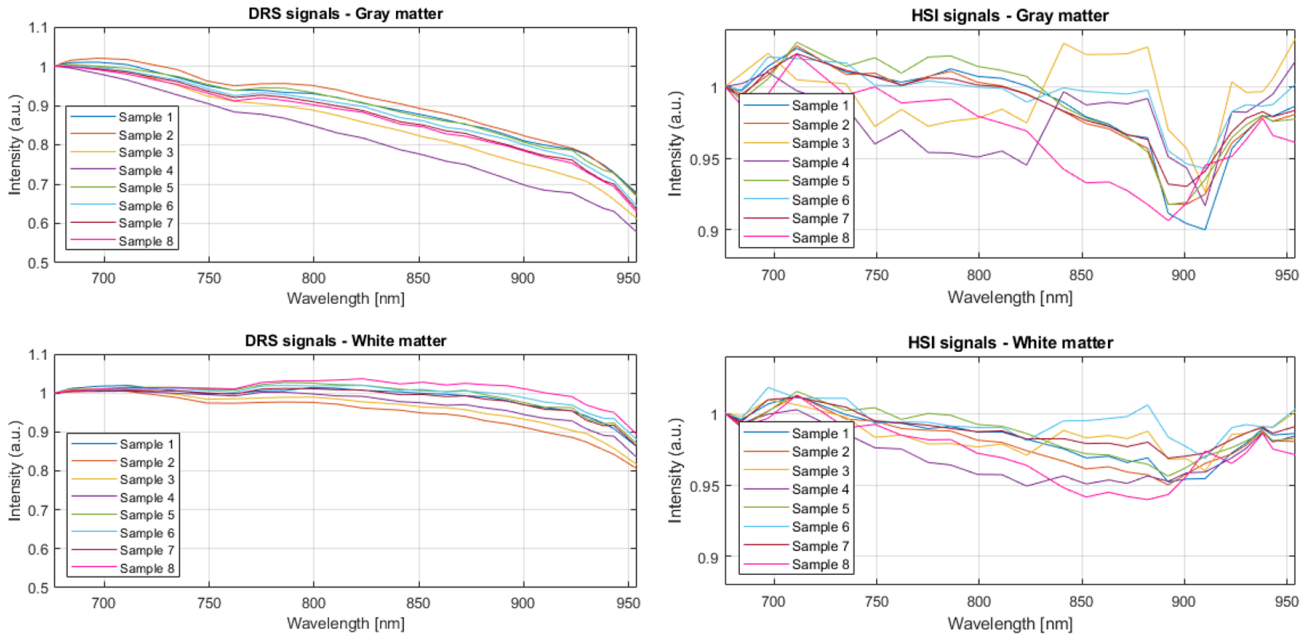

Figure 5: Averaged normalized signals of white and gray matter of the eight brain samples, both for DRS and HSI.

4. DISCUSSION

In these experiments, we have explored the potential of automated porcine brain-tissue classification using DRS and HSI technologies, extracting spectral features from the near-infrared range. DRS performs very well with a well-balanced sensitivity and specificity. This is possible since the shapes of the DRS signals are highly conform and appear with a very low variance, both for gray and white matter. For the HSI signals, however, sensitivity

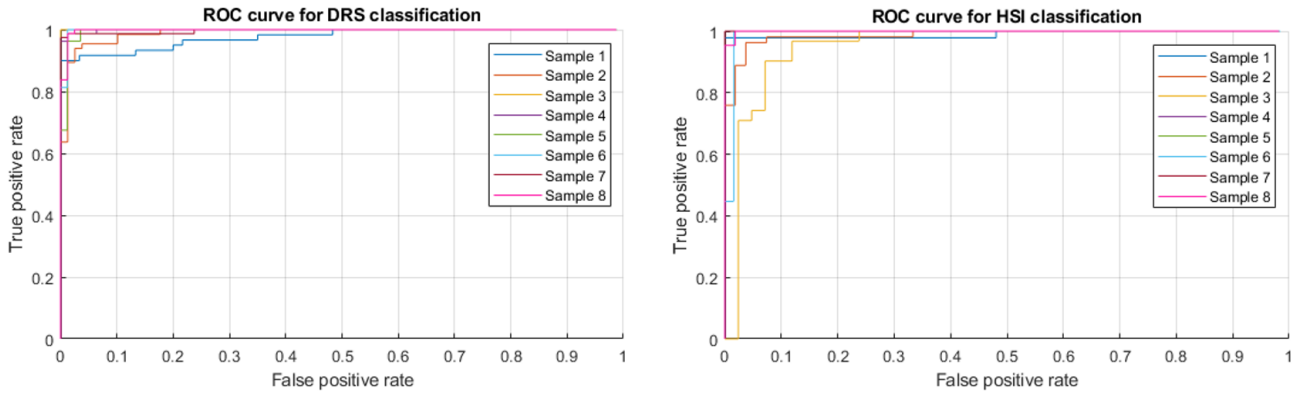

Figure 6: ROC curves for the eight brain samples with SVM classification, for DRS and HSI.

	DRS			HSI		
	AUC	**Sens.**	**Spec.**	**AUC**	**Sens.**	**Spec.**
Sample 1	0.93	0.92	0.95	0.91	0.76	1
Sample 2	0.93	0.95	0.91	0.96	0.96	0.96
Sample 3	0.99	0.98	1	0.85	1	0.69
Sample 4	0.96	0.91	1	0.98	1	0.96
Sample 5	0.93	1	0.85	0.99	0.98	1
Sample 6	0.99	0.99	0.99	0.96	0.91	0.98
Sample 7	0.98	0.96	1	1	1	1
Sample 8	0.98	1	0.95	0.93	1	0.87
Mean	0.96	0.96	0.96	0.95	0.95	0.93

Table 1: Performance comparison between classification with DRS and HSI.

reaches 95%, similar to DRS, but specificity becomes 93%, with the lowest classification score obtained for Sample 3 (Sp 69%) and Sample 8 (Sp 87%). As mentioned in Section 3, the shape of the signal of these two Samples (3 and 8) is much different than the other samples. White and gray matter have different composition that can be captured by both infrared sensing techniques, which results in a good accuracy when automated tissue classification is performed. This feasibility study represents a first step towards real-time tumor detection and classification for clinical use.

There is another aspect that should be considered about DRS and HSI. Whereas DRS is a spot measurement which requires contact with the tissue for spectral signature acquisition, HSI is a contactless imaging technique that can be used in real-time operation during surgery. Although HSI shows less smooth behavior in the spectrum, with normalization, we were able to achieve a reliable spectral measurement that can be classified automatically. Moreover, HSI has been already exploited for *ex-vivo* tissue classification and cancer detection,[7,8] while research is now moving towards real-time neurosurgical operations.[12] By coupling the HSI sensor to the endoscope, we aimed to design a prototype of an endoscopic system that can perform tissue classification, which may be used in the future during minimally invasive neurosurgical procedures, thereby increasing the information available for the surgeons.

5. CONCLUSIONS

In this study, we explore the potential of automated porcine brain-tissue classification with DRS and HSI, by extracting spectral features from the near-infrared range. The classification employs linear support vector machine and is performed on eight *ex-vivo* porcine brain-tissue samples, which are analyzed and classified as either white or gray matter. The DRS combined with the proposed classification reaches sensitivity and specificity of 96%, while HSI reaches a sensitivity of 95% and specificity of 93%. The results show that the spectral signature

of the tissue in the near-infrared range contains enough information to automatically discriminate brain tissue in white and gray matter. Thus far, we have classified healthy tissue in white and gray matter, but the primary objective will be to use this technology for real-time classification of healthy and tumor tissue during surgery. This feasibility study shows the potential of DRS and HSI for tissue classification and paves the way for a further investigation towards real-time clinical brain tumor detection deeper inside tissue.

ACKNOWLEDGMENTS

The first author greatfully acknowledges the funding from the European Horizon 2020 research and innovation programme under the Marie Skłodowska-Curie grant agreement No.: 721766 (FBI).

REFERENCES

[1] Fabelo, H., Ortega, S., Lazcano, R., Madroñal, D., M Callicó, G., Juárez, E., Salvador, R., Bulters, D., Bulstrode, H., Szolna, A., et al., "An intraoperative visualization system using hyperspectral imaging to aid in brain tumor delineation," *Sensors* **18**(2), 430 (2018).

[2] Swamy, A., Burström, G., Spliethoff, J. W., Babic, D., Reich, C., Groen, J., Edström, E., Terander, A. E., Racadio, J. M., Dankelman, J., et al., "Diffuse reflectance spectroscopy, a potential optical sensing technology for the detection of cortical breaches during spinal screw placement," *Journal of biomedical optics* **24**(1), 017002 (2019).

[3] Evers, D., Hendriks, B., Lucassen, G., and Ruers, T., "Optical spectroscopy: current advances and future applications in cancer diagnostics and therapy," *Future oncology* **8**(3), 307–320 (2012).

[4] Spliethoff, J. W., Tanis, E., Evers, D. J., Hendriks, B. H., Prevoo, W., and Ruers, T. J., "Monitoring of tumor radio frequency ablation using derivative spectroscopy," *Journal of biomedical optics* **19**(9), 097004 (2014).

[5] Lu, G. and Fei, B., "Medical hyperspectral imaging: a review," *Journal of biomedical optics* **19**(1), 010901 (2014).

[6] Halicek, M., Fabelo, H., Ortega, S., Little, J. V., Wang, X., Chen, A. Y., Callico, G. M., Myers, L. L., Sumer, B. D., and Fei, B., "Cancer detection using hyperspectral imaging and evaluation of the superficial tumor margin variance with depth," in [*Medical Imaging 2019: Image-Guided Procedures, Robotic Interventions, and Modeling*], **10951**, 109511A, International Society for Optics and Photonics (2019).

[7] Fabelo, H., Ortega, S., Ravi, D., Kiran, B. R., Sosa, C., Bulters, D., Callicó, G. M., Bulstrode, H., Szolna, A., Piñeiro, J. F., et al., "Spatio-spectral classification of hyperspectral images for brain cancer detection during surgical operations," *PloS one* **13**(3), e0193721 (2018).

[8] Manni, F., van der Sommen, F., Zinger, S., Kho, E., de Koning, S. B., Ruers, T., Shan, C., Schleipen, J., et al., "Automated tumor assessment of squamous cell carcinoma on tongue cancer patients with hyperspectral imaging," in [*Medical Imaging 2019: Image-Guided Procedures, Robotic Interventions, and Modeling*], **10951**, 109512K, International Society for Optics and Photonics (2019).

[9] Lu, G., Wang, D., Qin, X., Muller, S., Wang, X., Chen, A. Y., Chen, Z. G., and Fei, B., "Detection and delineation of squamous neoplasia with hyperspectral imaging in a mouse model of tongue carcinogenesis," *Journal of biophotonics* **11**(3), e201700078 (2018).

[10] Fei, B., Lu, G., Wang, X., Zhang, H., Little, J. V., Patel, M. R., Griffith, C. C., El-Diery, M. W., and Chen, A. Y., "Label-free reflectance hyperspectral imaging for tumor margin assessment: a pilot study on surgical specimens of cancer patients," *Journal of biomedical optics* **22**(8), 086009 (2017).

[11] Lu, G., Qin, X., Wang, D., Muller, S., Zhang, H., Chen, A., Chen, Z. G., and Fei, B., "Hyperspectral imaging of neoplastic progression in a mouse model of oral carcinogenesis," in [*Medical Imaging 2016: Biomedical Applications in Molecular, Structural, and Functional Imaging*], **9788**, 978812, International Society for Optics and Photonics (2016).

[12] Fabelo, H., Ortega, S., Kabwama, S., Callico, G. M., Bulters, D., Szolna, A., Pineiro, J. F., and Sarmiento, R., "Helicoid project: A new use of hyperspectral imaging for brain cancer detection in real-time during neurosurgical operations," in [*Hyperspectral Imaging Sensors: Innovative Applications and Sensor Standards 2016*], **9860**, 986002, International Society for Optics and Photonics (2016).